JACS
JOURNAL OF THE AMERICAN CHEMICAL SOCIETY
Article
pubs.acs.org/JACS

Sequence Effects on Peptide Assembly Characteristics Observed by Using Scanning Tunneling Microscopy

Xiaobo Mao,[†,§] Yuanyuan Guo,[†,§] Yin Luo,[‡,§] Lin Niu,[†] Lei Liu,[†] Xiaojing Ma,[†] Huibin Wang,[†] Yanlian Yang,*[,†] Guanghong Wei,*[,‡] and Chen Wang*[,†]

[†]National Center for Nanoscience and Technology, 11 Beiyitiao Zhongguancun, Beijing 100190, China

[‡]State Key Laboratory of Surface Physics, Key Laboratory for Computational Physical Sciences (Ministry of Education), and Department of Physics, Fudan University, 220 Handan Road, Shanghai 200433, China

Supporting Information

ABSTRACT: Homogeneous assemblies of the model peptides at interfaces have been achieved and observed with scanning tunneling microscopy. The dependence of the observed brightness in STM images is analyzed, and the correlation with the peptide residues is proposed. We have also investigated the conformational dynamics of the peptide assemblies adsorbed on a graphene sheet by performing all-atom molecular dynamic simulations in water at 300 K. The simulation results of the two peptide assemblies on graphite surfaces show that $R_4G_4H_8$ and $F_4G_4H_8$ peptide assemblies are mostly in β-sheet structure, and the interaction energy of the four different residues with graphite surfaces follows the order of Phe > His > Arg > Gly, consistent with their brightness contrasts in STM images. The insight on the distribution of residue moieties in the peptide assemblies could provide beneficial venues for studying peptide-based interfacial processes such as site-specific interactions between molecular species with peptides.

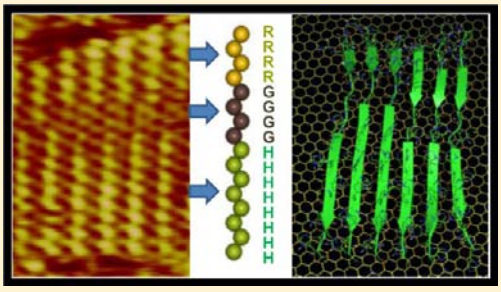

INTRODUCTION

Molecularly resolved structural insight of peptide assemblies has been recently demonstrated with scanning tunneling microscopy (STM) operated in both ultrahigh vacuum (UHV) and ambient conditions.[1−5] This progress has generated complementary insight into the peptide interactions leading to various forms of peptide aggregates relevant to neurodegenerative diseases. While STM has been demonstrated as an effective approach to study the noncrystalline peptide assemblies that are in general challenging for X-ray diffraction and solid-state nuclear magnetic resonance, a number of very interesting issues remain open such as identification of amino acid residues and models with atomic specificity in peptide assemblies, etc. These aspects should be keen to advance the understanding of the fundamental aspects in peptide interactions and assemblies relating to various degenerative diseases.

It is worth mentioning that the submolecular structural characteristics of the peptide assemblies could be correlated with the adsorption conformation, electron density of states of peptide moieties etc. High-resolution STM images have shown the individual residues on the peptide chains, and the results revealed the heterogeneities at the submolecule level and dynamic changes of residue conformations.[6] It can be envisioned that such progress could enable studies on the amino acid sequence effects on biologically relevant peptide assemblies using STM.

The dominant interactions in peptide assemblies could be contributed jointly from peptide backbones and residues. Hydrogen bonds between amine moieties of peptide chains are known significant for peptide assemblies. In addition, rich varieties of interactions between residue moieties could also have significant contributions depending on the chemical nature of the residues, that is, electrostatic, hydrogen-bonding, hydrophobic, and steric interactions. Particularly, for surface-bound peptides, the adsorption conformation of residues reflects the molecule−substrate interactions.

In this study, we endeavored to analyze the characteristics of the peptide assemblies on surfaces in ambient conditions, particularly the correlation between the brightness contrast in STM images and specific residue groups. We studied two synthetic model peptides, $R_4G_4H_8$ and $F_4G_4H_8$, containing four kinds of residue groups (Phe-benzyl, Arg-carbamidine, Gly-hydrogen, and His-imidazole), representing typical types of interactions between residues. Our study illustrates that these residues could be qualitatively differentiated according to the observed brightness contrasts and the ordering of the assemblies on the surface. The molecular dynamic (MD) simulations based on STM results help reveal the molecular mechanism of the observed assembly conformations.

MATERIALS AND METHODS

Sample Preparation. Synthetic peptides $R_4G_4H_8$ and $F_4G_4H_8$ (Scheme 1) were obtained from Shanghai Bootech Bioscience Co., Ltd. The purity of the peptides (>98%) has been verified by high-

Received: July 26, 2012
Published: January 18, 2013

   dx.doi.org/10.1021/ja307198u | J. Am. Chem. Soc. 2013, 135, 2181−2187

Scheme 1. Abbreviation and Molecular Structures of the Designed Peptides: $R_4G_4H_8$ and $F_4G_4H_8$

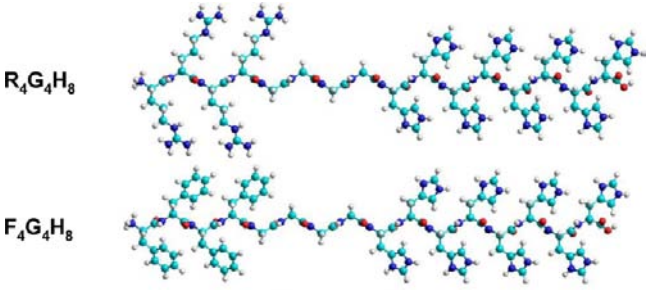

performance liquid chromatography and mass spectrum analyses. All of the materials were purchased and used without further purification.

Lyophilized powders of peptides were respectively dissolved in Milli-Q water into a concentration of 1 mg/mL. The peptide solutions (15 μL) were deposited on the surface of freshly cleaved highly oriented pyrolytic graphite (HOPG) for 1 min incubation. After that, the excess solution was blown away from the HOPG surfaces and blown dry by using high-purity nitrogen gas prior to STM experiments.

STM Experiments. STM experiments were performed in constant-current mode under ambient conditions (Nanoscope IIIa SPM system, Bruker Nano, USA). The STM tips were mechanically formed by Pt/Ir wire (80/20). The tunneling conditions are described in the corresponding figure captions. Experiments were repeated independently using different tips for reproducibility.

Molecular Dynamics Simulations. Molecular dynamics (MD) simulations were carried out using the GROMACS 4.5.3 package[7] with GROMOS96 43a1 force field.[8] The bonded and nonbonded parameters of graphite sheet were taken from previous studies by Koumoutsakos et al.[9] and Hummer et al.,[10] respectively. The initial states of $F_4G_4H_8$ and $R_4G_4H_8$ are eight-stranded in-register parallel β-sheets. The graphite sheet is 7.6 nm × 7.6 nm in size, which provides sufficient surface for the β-sheet to adsorb. In the initial configuration, the minimum distance between the peptide β-sheet and graphite sheet is 1.4 nm. The $F_4G_4H_8$–graphite system and the $R_4G_4H_8$–graphite system were solvated in a 7.6 nm × 7.6 nm × 3.8 nm and a 7.6 nm × 7.6 nm × 4.4 nm SPC (simple point charge model)[11] water box, respectively. The total number of water molecules in the two different systems is 5939 and 6862, respectively. Two independent 100 ns MD simulations were performed for each system at 300 K in isothermal–isobaric (NPT) ensemble. The solute and solvent were separately coupled to external temperature bath using velocity rescaling method[12] and pressure bath using Parrinello–Rahman method.[13] The temperature and the pressure were maintained at 300 K and 1 bar using coupling constants of 0.1 and 1.0 ps, respectively. Bond lengths within peptides and water molecules were respectively constrained by the LINCS[14] and the SETTLE algorithms,[15] allowing an integration time step of 2 fs. Particle mesh Ewald method was used to calculate the electrostatic interaction with a real space cutoff of 0.9 nm, and the van der Waals interactions were calculated using a cutoff of 1.4 nm. All MD simulations were performed using periodic boundary conditions. The position of graphite sheet was fixed during all of the MD simulations.

RESULTS AND DISCUSSION

Typical peptide assemblies such as amyloid-β[16] and amylin[3,5] have been studied using STM with the core β-sheet structures and folding sites resolved. It may be recognized that peptide lamellae with diverse brightness contrasts in STM images could further provide a unique opportunity to analyze the adsorbed peptide structures and binding regions of possible inhibitors at single amino acid level. In this work, we explore the correlation between the brightness contrast and specific residue groups on the basis of two model peptides $R_4G_4H_8$ and $F_4G_4H_8$, which could manifest the representative interactions for amino acids.

The STM image of $R_4G_4H_8$ assembly structures on graphite surfaces is shown in Figure 1A, with bright lamellae attributed

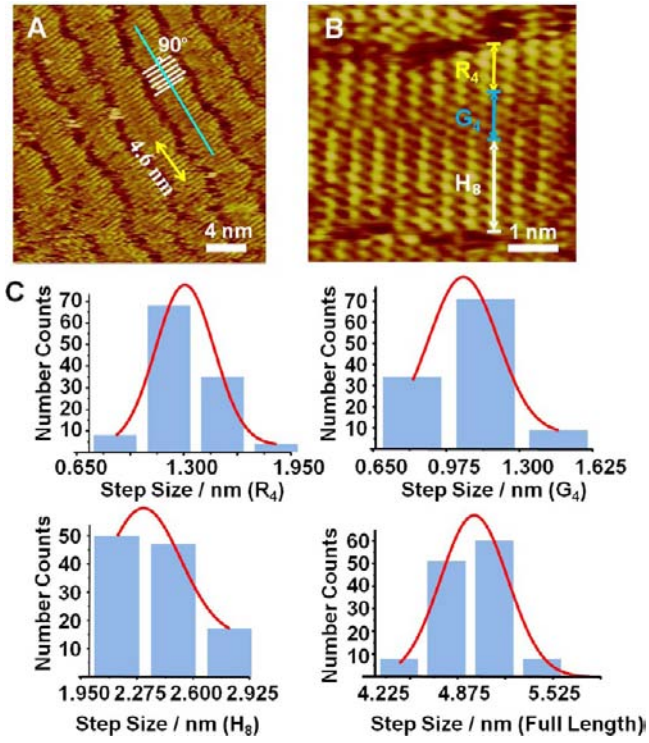

Figure 1. STM images of $R_4G_4H_8$ assembly and the statistical analysis of the measured lengths. (A) Large-scale STM image of $R_4G_4H_8$. The length of the yellow arrow, covering 10 molecules, is 4.6 nm. The molecular axes of peptides (a group of short white lines) are perpendicular to the long axis of the stripe (cyan line). (B) High-resolution STM image of $R_4G_4H_8$. R_4, G_4, and H_8 are marked by yellow, blue, and white arrows, respectively. Tunneling conditions: (A) I = 332.3 pA, V = 698.6 mV; (B) I = 307.5 pA, V = 773.2 mV. (C) Statistical histograms of the length of $R_4G_4H_8$ molecules. The most probable values given are determined from the Gaussian function (red lines) from the peptide length statistical results. R_4 = 1.2 ± 0.2 nm, G_4 = 1.0 ± 0.2 nm, H_8 = 2.4 ± 0.2 nm, full-length is 4.9 ± 0.6 nm. The step size (0.325 nm) is the length increment of every residue in the parallel β-sheet structures.

to assembled peptides. In the lamellae, the three bands with different brightness contrasts are consistent in length with the designed sequence $R_4G_4H_8$. The molecular axes of peptides $R_4G_4H_8$ (as highlighted by white lines) are approximately perpendicular to the long axes of the stripes (as highlighted by a cyan line).

The averaged separation between two neighboring peptide strands in the STM images is 4.6 ± 0.2 Å[3,17] (indicated by yellow arrows in Figure 1A), which is in good agreement with the strand-to-strand distance of characteristic β-sheet structures, and indicative of the formation of β-sheet structures. The β-sheet structures could be confirmed by Fourier transform infrared (FTIR) spectroscopy, in which amide I frequencies of peptides are located around 1640–1615 cm^{-1}. Furthermore, the absence of a band at >1680 cm^{-1} suggests the parallel stacking of β-sheet.[18,19] The strong band located at 1633 cm^{-1} without a band above 1680 cm^{-1} was observed in the FTIR

dx.doi.org/10.1021/ja307198u | J. Am. Chem. Soc. 2013, 135, 2181–2187

spectrum of $R_4G_4H_8$ assembly, confirming the parallel β-sheet structures (Figure S1A).

In the high-resolution STM image (Figure 1B), it can be clearly resolved that the consisting bands of the lamellae appear with different width. On the basis of the peptide sequence, R_4 may plausibly represent the narrow band with relatively high contrast (as highlighted by yellow arrows in Figure 1B), G_4 may represent the narrow band with low contrast (as highlighted by blue arrows), and H_8 may represent the relatively wide band (as highlighted by white arrows).

The widths of the bands with different brightness are measured, and the histograms are provided. The definition and criteria for the width measurements have been reported in our previous work,[3] which are defined as the lengths of the dotted stripe-shaped features with three contrasts (Figure S2A and B). The three different segments are separated by the abrupt slope changes in the sectional profile (Figure S2C and D). Because of the contrast variations in the peptide strands, the uncertainty of the width measurement on different segments is inevitable, while the fidelity is based on the identical criteria in all of the width measurements. The width analysis (Figure 1C and Table S1) further confirms the correlation between the brightness contrast and the peptide sequence of $R_4G_4H_8$. The red lines in the histogram stand for Gaussian fitting for the peptide length distribution. The step size (0.325 nm) is the length increment of every residue in the parallel β-sheet structures, which could be assumed in the statistical histogram of the width distribution of peptide lamellae. The histogram of the length distribution of $R_4G_4H_8$ molecules indicates that the most probable peptide length is 4.9 ± 0.6 nm, which is slightly shorter than the fully extended peptide strands (5.2 nm for 16-mer peptide assuming 0.325 nm per residue). The width of the narrow bright band corresponding to R_4 is 1.2 ± 0.2 nm. The measured width of R_4 band is about 24.5% of the full-length of $R_4G_4H_8$, which is close to the expected value of 25% in the peptide sequence. The width of the low contrast band corresponding to G_4 in the middle of lamellae is 1.0 ± 0.2 nm, taking up 20.4% of full-width. The average width of the band with high brightness contrast corresponding to H_8 is 2.4 ± 0.2 nm accounting for 49.0% of $R_4G_4H_8$. The proportion of the widths of three bands is approximately 1.2:1:2.4 by brightness contrast, which is consistent qualitatively with the designed sequence ratio. On the basis of the length distribution of the designed sequence and the brightness contrast from STM images, we therefore propose that peptide $R_4G_4H_8$ forms parallel β-sheet-like assembly structures. Brightness contrasts from STM images are related to specific amino acid moieties (guanidine, hydrogen, and imidazole) in the $R_4G_4H_8$ assemblies.

It is noticeable that the bright regions of R_4 and H_8 are not in line in Figure 1B STM image. The contribution to the observed brightness in STM images is jointly from the residues and the backbones, as well as the adsorbed conformation. The alignment of the peptides in the assemblies is greatly affected by the interpeptide interactions, which can originate from van der Waals, hydrogen bond, and electrostatic forces. Such multiplicity of interpeptide interactions could plausibly lead to polymorphic assembly configurations as reflected in slight alignment variations in the observed images. A recent report by Linderoth et al. on the assembly of tetra-peptide reveals that the bright region of the peptide KVVE is L-shaped, and the Lys residues are not strictly aligned with other residues.[6]

In the parallel study, we examined another model peptide $F_4G_4H_8$ and also observed the similar assembly feature with bands of varied brightness contrast (Figure 2A and B). The molecular axes of peptides $F_4G_4H_8$ are approximately

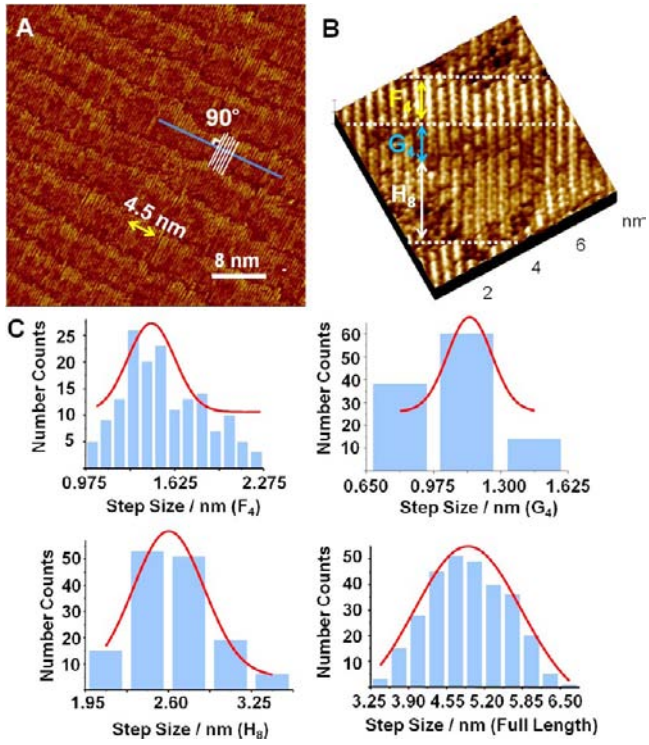

Figure 2. STM images of $F_4G_4H_8$ assembly and the statistical analysis of the measured lengths. (A) Large-scale STM image of $F_4G_4H_8$. The length of the yellow arrow, covering 10 molecules, is 4.5 nm. The molecular axes of peptides (a group of short white lines) are perpendicular to the long axis of the stripe (blue line). (B) High-resolution STM image of $F_4G_4H_8$. The brightest band (F_4) is marked by yellow arrows, and the rest of the bands (G_4 and H_8) are marked by blue and white arrows. Tunneling conditions: (A) I = 347.3 pA, V = −506.8 mV. (B) I = 521.7 pA, V = −450.0 mV. (C) Statistical histograms of the length of $F_4G_4H_8$ molecules. The most probable values given are determined from the Gaussian function (red lines) from the peptide length statistical results. F_4 = 1.4 ± 0.2 nm, G_4 = 1.1 ± 0.2 nm, H_8 = 2.6 ± 0.3 nm, full-length is 4.9 ± 0.9 nm. The step size (0.325 nm) is the length increment of every residue in the parallel β-sheet structures.

perpendicular to the long axes of the stripes, and the averaged separation between two neighboring molecules is 4.5 Å, which could be also indicative of the β-sheet structure considering the band located at 1631 cm^{-1} for parallel β-sheet formation (Figure S1B). The histogram of the width distribution of $F_4G_4H_8$ lamellae shows that the full-length peptide is 4.9 ± 0.9 nm and the brightest band is 1.4 ± 0.2 nm in width. The brightest band observed accounts for 28.6% of the peptide full-length (Figure 2C and Table S2), which can be attributed to F_4 (as marked by the yellow arrows). The width of the low contrast band corresponding to G_4 (as marked by the blue arrows) in the middle of lamellae is 1.1 ± 0.2 nm, taking up 22.4% of full-length. The average width of the high contrast band corresponding to H_8 (as marked by white arrows) is 2.6 ± 0.2 nm accounting for 53.0% of $F_4G_4H_8$. The proportion of the widths of three bands is approximately 1.3:1:2.4 by brightness contrast, which is consistent qualitatively with the designed peptide sequence ratio, related to specific amino acid moieties (benzyl, hydrogen, and imidazole). We also measured the

dx.doi.org/10.1021/ja307198u | J. Am. Chem. Soc. 2013, 135, 2181−2187

brightness intensity of each type of residue from both $R_4G_4H_8$ and $F_4G_4H_8$ STM images. Because the H_8 repeats in two peptides and the brightness contrast is medium in magnitude (higher than G_4 as the standard), the H_8 is chosen as a reference for normalizing the brightness intensities. In the STM study, the absolute height magnitude is dependent on the imaging conditions, such as tip geometry and bias conditions. To compare the contributions from different residues, the relative brightness for the peptide segments of R/H and F/H has been presented in percentage after normalization (Figure 3)

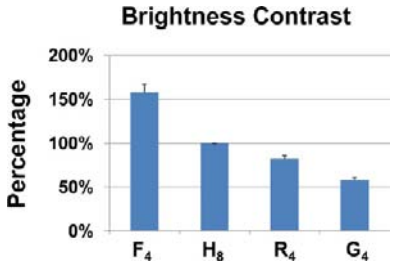

Figure 3. The brightness contrast comparison of four regions from two peptides in STM images. We use the Nanoscope program to measure relative heights of four regions (F_4, R_4, G_4, and H_8) and do normalization with H_8 as standard reference. The brightness sequence is F_4 (158%) > H_8 (100%) > R_4 (82%) > G_4 (58%).

as F_4 (158%) > H_8 (100%) > R_4 (82%) > G_4 (58%), which provides a venue to evaluate the brightness dependence on different amino acid residues. Because the STM contrast is sensitively dependent on the bias voltage and polarity, the STM images and brightness contrast comparison charts, as well as the absolute value for brightness in STM images, have been obtained at different bias conditions and reversed polarity (Figures S3 and S4). We did observe noticeable brightness variations at different bias and polarity, while the contrast difference between different bands is qualitatively reproducible at different bias conditions. We have also noticed significant brightness changes in terminal regions as illustrated in this figure, which is a clear indication that the residues in the current study may not be sufficiently rigid in adsorption conformation under scanning conditions. It should be noted that to obtain rigorous observation of the brightness dependence on bias voltage and polarity, it is critical to have sufficient adsorption stability of the molecular moieties as documented in numerous previous STM studies on single organic molecules under ultra high vacuum and low temperatures or molecular assemblies. However, we believe it is plausible to make reliable comparisons for the observed brightness for different residues under identical imaging conditions within individual STM image as in the current study. We wish also to note here that to perform reliable analysis of the brightness of the residues under different imaging conditions, serious efforts should be needed to enhance the adsorption stability of peptides.

Because $F_4G_4H_8$ contains two kinds of simple aromatic ring (benzyl, imidazole) in the residue groups at each side of molecular chain, it is interesting to explore the difference in the adsorption conformations between the two specific residues (F_4 and H_8) in peptide assemblies on graphite surfaces. To examine the atomic details of the $R_4G_4H_8$ and the $F_4G_4H_8$ assemblies at graphite surfaces, we carried out two independent 100 ns MD simulations for each system at 300 K. As our STM data reveal a β-sheet structure for the two peptides, to examine the structural stability of β-sheet, the initial state is a preformed monolayer β-sheet placed parallel to the graphite surface (see the snapshot at t = 0 ns in Figures 4 and 5). To allow the peptide side chains to

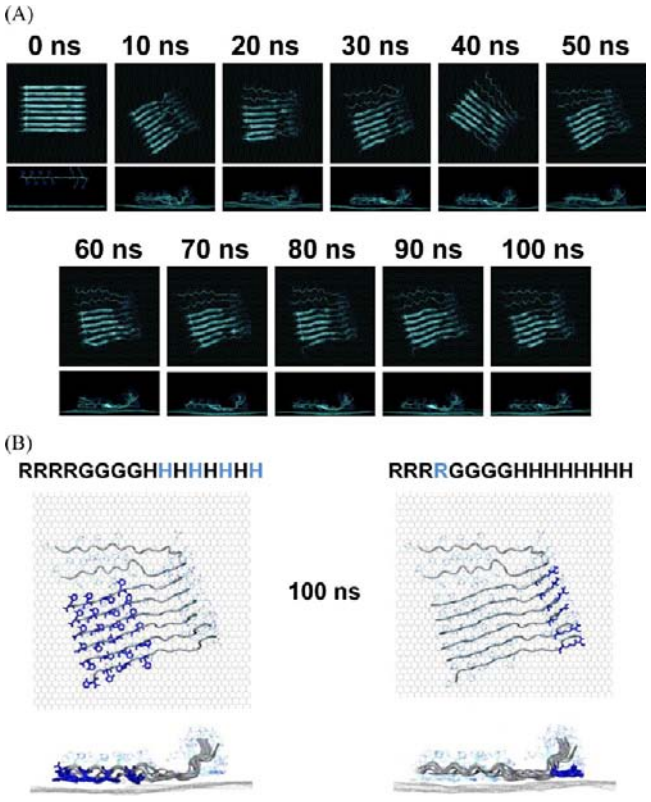

Figure 4. All-atom MD simulation results of $R_4G_4H_8$ assembly on graphite surface. (A) Snapshots at t = 0–100 ns, with $R_4G_4H_8$ in cartoon representation. (B) Top view and side view of $R_4G_4H_8$ assembly on graphite surface at t = 100 ns. The backbones and the side chains of $R_4G_4H_8$ are in cartoon and line representations, respectively. The side chains of residues R and H are highlighted by blue lines.

adjust their conformations prior to adsorption on the graphite surface, the minimum distance between the β-sheet and the graphite surface is 1.4 nm, that is, without any atomic contacts between peptide and surface. The simulation results for $R_4G_4H_8$ and $F_4G_4H_8$ systems are given in Figures 4 and 5, respectively. We first analyze the data for $R_4G_4H_8$ system. In the initial state, the imidazole rings of His residues are perpendicular to the graphite surface. With the increase of simulation time, the $R_4G_4H_8$ β-sheet began to move to the graphite surface (Figure 4A). At t = 10 ns, the G_4H_8 region adsorbed on the graphite surface, while the backbone of R_4 region bent upward with the long alkaline chain of residue Arg lying on the graphite surface. The H_8 segment remained in β-sheet structure, while the R_4G_4 region unfolded partially. This was followed by the unfolding of two strands at one edge of the β-sheet due to finite size effect. At t = 30 ns, these two strands almost completely unfolded, while the other six chains kept mostly β-sheet structure. In the left period of MD simulation, the $R_4G_4H_8$ assembly fluctuated around this conformation with the imidazole rings of His residues keeping parallel to the graphite surface (see Figure 4B). The simulation result (Figure 4B) also shows features similar to those of STM images (Figure 1B) that R_4 and H_8 bands are not in line in the assembly.

Similar analysis was made for the $F_4G_4H_8$ system (see Figure 5). At t = 0 ns, the $F_4G_4H_8$ β-sheet was placed parallel to the

dx.doi.org/10.1021/ja307198u | J. Am. Chem. Soc. 2013, 135, 2181–2187

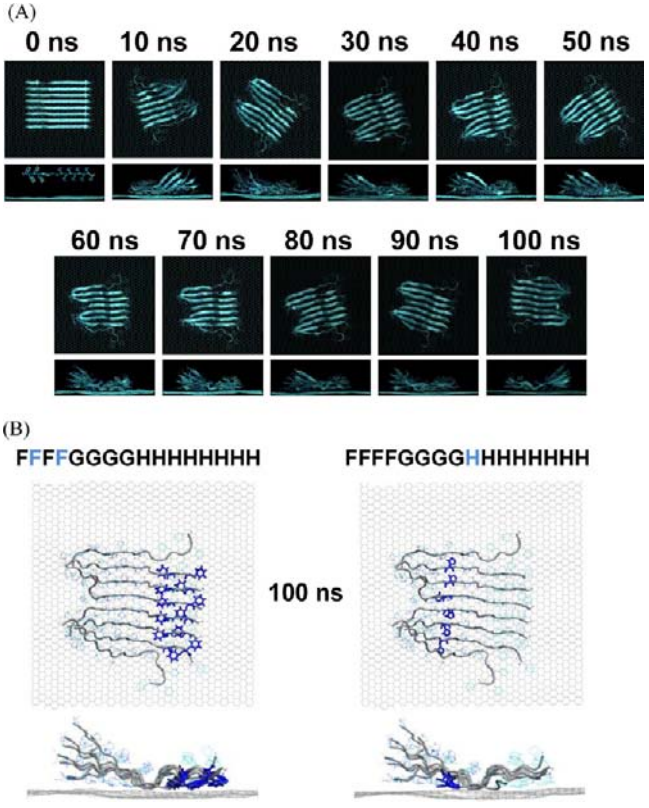

Figure 5. All-atom MD simulation results of $F_4G_4H_8$ assembly on graphite surface. (A) Snapshots at t = 0−100 ns, with $F_4G_4H_8$ in cartoon representation. (B) Top view and side view of $F_4G_4H_8$ assembly on graphite surface at t = 100 ns. The backbones and the side chains of $F_4G_4H_8$ are, respectively, in cartoon and line representations. The side chains of residues F and H are highlighted by blue lines.

graphite surface with a minimum peptide−graphite distance of 1.4 nm, and the aromatic rings of Phe residues were perpendicular to the graphite surface. After the MD run initiated, the $F_4G_4H_8$ β-sheet moved toward the graphite surface (Figure 5A). At t = 10 ns, F_4 preferentially adsorbed on the surface, while the H_8 still stayed in the aqueous solution. After that, F_4 gradually reorientated their side chains, and the H_8 gradually adsorbed on the surface. Finally, the aromatic rings of F_4 became parallel to the graphite surface (see the snapshot at t = 100 ns, Figure 5B). During the whole process of simulation, the G_4 region was prone to unfold, while the F_4 and H_8 both remained in the β-sheet structure.

The length distributions of peptides in $R_4G_4H_8$ and $F_4G_4H_8$ assemblies were also calculated. The peptide length is estimated by the end-to-end distance (the distance between the Cα atom of the first residue and that of the last residue). The probability density functions of the $R_4G_4H_8$ and $F_4G_4H_8$ lengths were presented in Figure S5. Two probability peaks are seen for each peptide, with a dominant peak centered at 4.40 nm for $R_4G_4H_8$ and at 4.86 nm for $F_4G_4H_8$. This indicates that on the graphite surface, $F_4G_4H_8$ peptide is more extended than $R_4G_4H_8$. The chain length distributions for $R_4G_4H_8$ and $F_4G_4H_8$ are 3.7−4.9 and 3.25−5.25 nm, respectively, in good agreement with the length distribution features derived from STM images.

As shown in Figures 4 and 5, the two peptides both adopt β-sheet conformations on graphite surface. Considering the definition of β-sheet structures,[20] it is natural to consider that the peptides are adsorbed on the graphite surface with the side groups in alternating configuration, and with one-half of the residues exposed to the substrate[21−23] while the others point to solvent. Such side-chain orientations allow the adjacent residues in the sequence to have different interaction strength with graphite surface. Residues whose side chain points to graphite would have much stronger interactions than the residues whose side chain points to solvent, thus leading to the interaction energies of the individual residue with graphite to vary alternatively. It is expected that the residues with side chains pointing to graphite surface would make a dominant contribution to the average residue−graphite interaction energy. As there are even number of residues for each species of amino acid residues in both $R_4G_4H_4$ and $F_4G_4H_8$, the average residue−graphite interaction energy can reasonably reveal the relative interaction strength of different amino acid residues with graphite. The residues at terminal positions indeed appear to have different interactions with the graphite surface. This should be understandable considering the possible difference in adsorption conformations for residues at terminal positions. On the other hand, the averaged height in STM image should be mainly contributed from the residues pointing away from

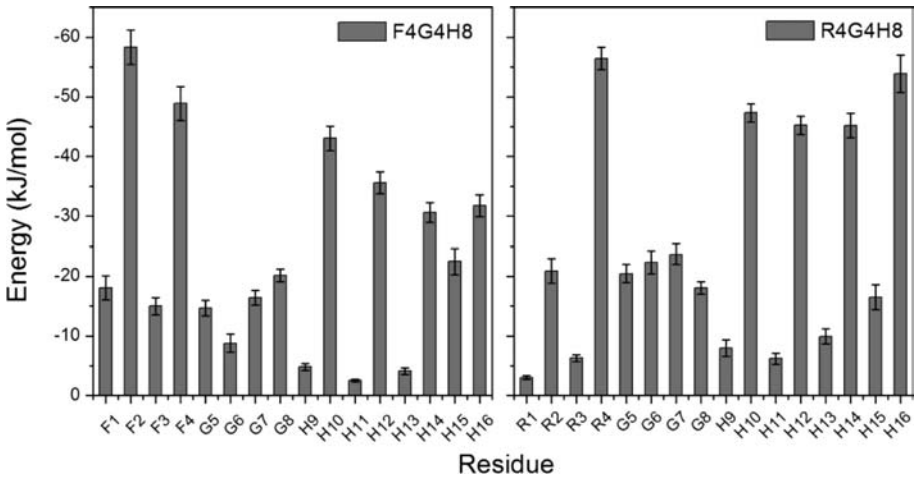

Figure 6. The interaction energy of each individual residue with graphene in $F_4G_4H_8$ (left panel) and $R_4G_4H_8$ (right panel) assemblies. The data are averaged over the last 50 ns of two independent 100 ns MD runs for each system.

dx.doi.org/10.1021/ja307198u | J. Am. Chem. Soc. 2013, 135, 2181−2187

graphite surface or to solvent. The magnitude of such average height should reflect the joint effect of the topographic feature and electronic structures of the residues as discussed above.

To explore the interaction strength of the two peptides with graphite surfaces, we plotted in Figure 6 the interaction energy as a function of amino acid residues. At first sight, the interaction energy of amino acid residue depends on the position of the residue in the amino acid sequence, and the same residue displayed different interaction energy with graphite surfaces. However, for each species of amino acid, when the interaction energy is averaged over the total number of amino acid residues, the residue−graphite interaction strength follows the trends: Phe > His > Arg > Gly. This is consistent with the brightness contrast of STM images shown in Figure 3, indicating that the brightness of the four different amino acid residues is correlated with their interaction energies with graphite surfaces. The contributing factors to the brightness of different amino acid residues can be considered as follows: the adsorption conformation of residues on graphite surfaces (that is, the physical locations of the amino acid residue groups and the peptide backbones) and the LDOS of the different residues. Because contribution from the peptide backbone is nearly the same both in chemical components and in extended zigzag configuration with β-sheet structures, the contribution to apparent brightness from the side groups would be dominant. Because of the higher LDOS for F and H residues with aromatic rings than R and G residues, the corresponding higher brightness contrast favors the preferential contribution from LDOS in comparison with the topographic effect. The topographic effect G_4 segments on image contrast should be dominant. In addition, one should note that the topographic effect (or adsorption conformation) is also directly related to the physical contact between the peptide segments and the graphite substrate. Such effect can be reflected in the interaction energy, which includes the contribution from both LDOS and adsorption conformation. The qualitative agreement between the interaction energy and the observed brightness contrast provides supportive evidence of the rationality of the above correlations.

The above effort suggests that identification of the specific residues in pristine peptide assemblies is promising and worthy of more rigorous investigations. In the present work, the short peptides with regular sequences are studied as model peptides for understanding the sequence effect on the peptide assembly structures. In principle, it should be applicable for peptides with longer and random residue sequences, especially the sequences in practical biological systems. However, because the brightness contrast is associated with the adsorption conformation of the peptides, and the local electronic structures of the residues, the expectation on rigorous structural resolution of less repetitive peptide sequence could be a nontrivial exploration.

CONCLUSIONS

In summary, the observed brightness contrast in STM images could help distinguish the residue groups in $R_4G_4H_8$ and $F_4G_4H_8$. Consistent with STM results, MD simulations show that the interaction energy of the four different residues with graphite surfaces follows the same order, that is, Phe > His > Arg > Gly, indicating that the brightness contrast of STM image is correlated with the interaction energies of the different residues with graphite surfaces. The measured neighboring-chain distance and the length distributions of the two peptides suggest that $R_4G_4H_8$ and $F_4G_4H_8$ both adopt parallel β-sheet structure on HOPG surfaces. This result is further supported by the structural stability of $R_4G_4H_8$ and $F_4G_4H_8$ β-sheets on graphite surfaces observed in two independent MD simulations. The correlation between the brightness contrasts with the peptide sequence and the related interaction energy may shed light on the sequence and conformation effects on the peptide assemblies. The insight on the distribution of residue moieties in the peptide assemblies could also provide beneficial venues for studying site-specific interactions between molecular species with peptides.

ASSOCIATED CONTENT

Supporting Information

Additional spectral data and peptide statistical length distributions. This material is available free of charge via the Internet at http://pubs.acs.org.

AUTHOR INFORMATION

Corresponding Author

wangch@nanoctr.cn; yangyl@nanoctr.cn; ghwei@fudan.edu.cn

Author Contributions

[§]These authors contributed equally.

Notes

The authors declare no competing financial interest.

ACKNOWLEDGMENTS

We thank Mr. Jonathan E. Nestor from Johns Hopkins University School of Medicine for his helpful discussion. This work was supported by the National Basic Research Program of China (2011CB932800, 2009CB930100). Financial support from the National Natural Science Foundation of China (NSFC, 91127043, 20911130229) and the Chinese Academy of Sciences (KJCX2-YW-M15) is also gratefully acknowledged. G.W. acknowledges the financial support from the NSFC (91227102 and 11074047).

REFERENCES

(1) Lingenfelder, M.; Tomba, G.; Costantini, G.; Ciacchi, L. C.; De Vita, A.; Kern, K. *Angew. Chem., Int. Ed.* **2007**, *46*, 4492−4495.

(2) Matmour, R.; De Cat, I.; George, S. J.; Adriaens, W.; Leclere, P.; Bomans, P. H. H.; Sommerdijk, N.; Gielen, J. C.; Christianen, P. C. M.; Heldens, J. T.; van Hest, J. C. M.; Lowik, D.; De Feyter, S.; Meijer, E. W.; Schenning, A. *J. Am. Chem. Soc.* **2008**, *130*, 14576−14583.

(3) Mao, X. B.; Wang, C. X.; Wu, X. K.; Ma, X. J.; Liu, L.; Zhang, L.; Niu, L.; Guo, Y. Y.; Li, D. H.; Yang, Y. L.; Wang, C. *Proc. Natl. Acad. Sci. U.S.A.* **2011**, *108*, 19605−19610.

(4) Mao, X. B.; Wang, Y. B.; Liu, L.; Niu, L.; Yang, Y. L.; Wang, C. *Langmuir* **2009**, *25*, 8849−8853.

(5) Mao, X. B.; Ma, X. J.; Liu, L.; Niu, L.; Yang, Y. L.; Wang, C. *J. Struct. Biol.* **2009**, *167*, 209−215.

(6) Kalashnyk, N.; Nielsen, J. T.; Nielsen, E. H.; Skrydstrup, T.; Otzen, D. E.; Lægsgaard, E.; Wang, C.; Besenbacher, F.; Nielsen, N. C.; Linderoth, T. R. *ACS Nano* **2012**, *6*, 6882−6889.

(7) Hess, B.; Kutzner, C.; van der Spoel, D.; Lindahl, E. *J. Chem. Theory Comput.* **2008**, *4*, 435−447.

(8) Van Gunsteren, W. F. B.; Eising, A. A.; Hünenberger, P. H.; Krüger, P.; Mark, A. E.; Scott, W. R. P.; Tironi, I. G. *Biomolecular Simulation: The GROMOS96 Manual and User Guide*; Biomos: Zürich, Switzerland, Groningen, Holland, 1996.

(9) Walther, J. H.; Jaffe, R.; Halicioglu, T.; Koumoutsakos, P. *J. Phys. Chem. B* **2001**, *105*, 9980−9987.

(10) Hummer, G.; Rasaiah, J. C.; Noworyta, J. P. *Nature* **2001**, *414*, 188−190.

(11) Berendsen, H. J. C.; Postma, J. P. M.; van Gunsteren, W. F.; Hermans, J. *Intermolecular Forces, Interaction Models for Water in*

Relation to Protein Hydration; D. Reidel Publishing Co.: Dordrecht, the Netherlands, 1981; pp 331−342.
(12) Bussi, G.; Donadio, D.; Parrinello, M. *J. Chem. Phys.* **2007**, *126*, 014101.
(13) Parrinello, M.; Rahman, A. *J. Appl. Phys.* **1981**, *52*, 7182−7190.
(14) Miyamoto, S.; Kollman, P. A. *J. Comput. Chem.* **1992**, *13*, 952−962.
(15) Hess, B.; Bekker, H.; Berendsen, H. J. C.; Fraaije, J. G. E. M. *J. Comput. Chem.* **1997**, *18*, 1463−1472.
(16) Ma, X.; Liu, L.; Mao, X.; Niu, L.; Deng, K.; Wu, W.; Li, Y.; Yang, Y.; Wang, C. *J. Mol. Biol.* **2009**, *388*, 894−901.
(17) Sunde, M.; Serpell, L. C.; Bartlam, M.; Fraser, P. E.; Pepys, M. B.; Blake, C. C. F. *J. Mol. Biol.* **1997**, *273*, 729−739.
(18) Miyazawa, T.; Blout, E. R. *J. Am. Chem. Soc.* **1961**, *83*, 712−719.
(19) Hiramatsu, H.; Goto, Y. J.; Naiki, H.; Kitagawa, T. *J. Am. Chem. Soc.* **2005**, *127*, 7988−7989.
(20) Kabsch, W.; Sander, C. *Biopolymers* **1983**, *22*, 2577−2637.
(21) Mao, X. B.; Guo, Y. Y.; Wang, C. X.; Zhang, M.; Ma, X. J.; Liu, L.; Niu, L.; Zeng, Q. D.; Yang, Y. L.; Wang, C. *ACS Chem. Neurosci.* **2011**, *2*, 281−287.
(22) Mao, X. B.; Wang, C. X.; Ma, X. J.; Zhang, M.; Liu, L.; Zhang, L.; Niu, L.; Zeng, Q. D.; Yang, Y. L.; Wang, C. *Nanoscale* **2011**, *3*, 1592−1599.
(23) Wang, C. X.; Mao, X. B.; Yang, A. H.; Niu, L.; Wang, S. N.; Li, D. H.; Guo, Y. Y.; Wang, Y. B.; Yang, Y. L.; Wang, C. *Chem. Commun.* **2011**, *47*, 10638−10640.